Second stability in the ATF torsatron—Experiment and theory

J. H. Harris, E. Anabitarte, G. L. Bell, J. D. Bell, T. S. Bigelow, B. A. Carreras, L. A. Charlton, R. J. Colchin , E. C. Crume, N. Dominguez, J. L. Dunlap, G. R. Dyer, A. C. England, R. F. Gandy, J. C. Glowienka, J. W. Halliwell, G. R. Hanson, C. Hidalgo-Vera, D. L. Hillis, S. Hiroe, L. D. Horton, H. C. Howe, R. C. Isler, T. C. Jernigan, H. Kaneko, J. N. Leboeuf, D. K. Lee, V. E. Lynch, J. F. Lyon, M. M. Menon, R. N. Morris, M. Murakami, G. H. Neilson, V. K. Paré, D. A. Rasmussen, C. E. Thomas, T. Uckan, M. R. Wade, J. B. Wilgen, and W. R. Wing

Citation: Physics of Fluids B **2**, 1353 (1990); doi: 10.1063/1.859555
View online: http://dx.doi.org/10.1063/1.859555
View Table of Contents: http://scitation.aip.org/content/aip/journal/pofb/2/6?ver=pdfcov
Published by the AIP Publishing

Second stability in the ATF torsatron—Experiment and theory*

J. H. Harris,† E. Anabitarte,[a] G. L. Bell,[c] J. D. Bell,[b] T. S. Bigelow, B. A. Carreras, L. A. Charlton,[b] R. J. Colchin, E. C. Crume, N. Dominguez, J. L. Dunlap, G. R. Dyer, A. C. England, R. F. Gandy,[c] J. C. Glowienka, J. W. Halliwell, G. R. Hanson,[d] C. Hidalgo-Vera,[a] D. L. Hillis, S. Hiroe, L. D. Horton, H. C. Howe, R. C. Isler, T. C. Jernigan, H. Kaneko,[e] J. N. Leboeuf, D. K. Lee,[b] V. E. Lynch,[b] J. F. Lyon, M. M. Menon, R. N. Morris,[b] M. Murakami, G. H. Neilson, V. K. Paré, D. A. Rasmussen, C. E. Thomas,[d] T. Uckan, M. R. Wade,[d] J. B. Wilgen, and W. R. Wing

Oak Ridge National Laboratory, Oak Ridge, Tennessee 37831-8072

(Received 30 November 1989; accepted 21 February 1990)

Access to the magnetohydrodynamic (MHD) second stability regime has been achieved in the Advanced Toroidal Facility (ATF) torsatron [Fusion Technol. **10**, 179 (1986)]. Operation with a field error that reduced the plasma radius and edge rotational transform resulted in peaked pressure profiles and increased Shafranov shift that lowered the theoretical transition to ideal MHD second stability to $\beta_0 \approx 1.3\%$; the experimental β values ($\beta_0 \leqslant 3\%$) are well above this transition. The measured magnetic fluctuations decrease with increasing β, and the pressure profile broadens, consistent with the theoretical expectations for self-stabilization of resistive interchange modes. Initial results from experiments with the field error removed show that the pressure profile is now broader. These later discharges are characterized by a transition to improved ($\times$2–3) confinement and a marked change in the edge density fluctuation spectrum, but the causal relationship of these changes is not yet clear.

I. INTRODUCTION

The ideal magnetohydrodynamic (MHD) second stability regime[1-3] is important to the improvement of toroidal confinement in tokamaks and stellarators because it offers the possibility that anomalous transport might decrease with increasing $\beta \equiv 2\mu_0 p/B^2$ (the ratio of the plasma kinetic pressure to the magnetic pressure). The goal of second stability experiments[4-6] is to use the changes in the internal magnetic surface geometry (magnetic axis shift and flux surface shape) produced by the finite-β toroidal equilibrium to reduce (and ultimately reverse) the unfavorable curvature responsible for the MHD instabilities that are thought to limit the achievable plasma pressure (ballooning modes in tokamaks, and interchange modes in stellarators).

In this paper we describe experiments on the Advanced Toroidal Facility (ATF) torsatron[7] (a type of stellarator) in which operation in the ideal MHD second stability regime was achieved at relatively low β by virtue of peaked pressure profiles resulting from the effects of a field error. In Sec. II we describe the mechanism of β self-stabilization of interchange modes in sheared stellarators. The results of the second stability studies for plasmas with the peaked pressure profiles are described in Sec. III. In Sec. IV, we present the first observations regarding fluctuations and confinement in the plasmas with broader pressure profiles that have been obtained in ATF since the field error was repaired, and Sec. V contains a summary of our conclusions.

II. SECOND STABILITY IN STELLARATORS—BACKGROUND

Figure 1 illustrates schematically the concepts of second stability and self-stabilization. For a given magnetic configuration, different sequences of finite-β equilibria can be selected using a control parameter such as the indentation of a bean-shaped tokamak[8] or the shift of the vacuum field magnetic axis in a sheared stellarator.[5] For a range of values of the control parameter, the plasma passes through a region of

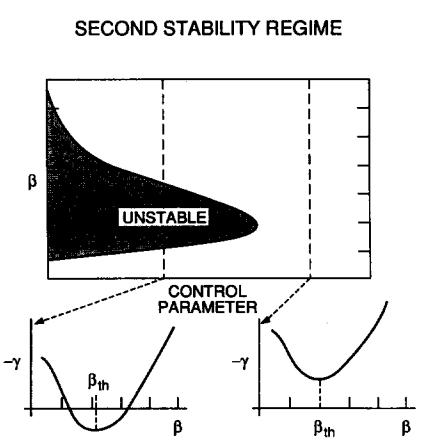

FIG. 1. Schematic illustration of ideal MHD second stability. Here γ is the ideal MHD growth rate. For the equilibrium sequence on the left, the plasma passes through a region of instability before entering the second stability regime. For the sequence on the right, the plasma passes directly into the regime where self-stabilization occurs.

* Paper 4I2, Bull. Am. Phys. Soc. **34**, 2000 (1989).

† Invited speaker.

[a] Permanent address: Centro de Investigaciones Energeticas, Medio Ambientales, y Tecnologicas (CIEMAT), Madrid, Spain.

[b] Permanent address: Computing and Telecommunications Division, Martin Marietta Energy Systems, Inc., Oak Ridge, Tennessee 37831.

[c] Permanent address: Auburn University, Auburn, Alabama 36849.

[d] Permenant address: Georgia Institute of Technology, Atlanta, Georgia 30332.

[e] Permanent address: Plasma Physics Laboratory, Kyoto University, Kyoto, Japan.

 0899-8221/90/061353-06$02.00

ideal MHD instability as β increases (leftmost dotted path in Fig. 1) and then becomes ideally stable as the finite pressure reduces the curvature drive. For other values of the control parameter, the plasma avoids the region of instability but still becomes more stable (γ becomes more negative) as β increases past a transition value.

Because of their external control of magnetic configuration and the absence of plasma current, stellarators are well suited for exploring the second stability regime and studying β self-stabilization. In stellarators with significant positive shear in the rotational transform ($d\iota/dr > 0$, where ι is the rotational transform and r is the plasma minor radius), the dominant instabilities[5] are interchange modes that occur when there is a sufficient pressure gradient on a surface of rational ι that lies in a region of unfavorable average magnetic curvature or "magnetic hill" where $V'' > 0$. (Here the specific volume V' is the asymptotic value of the field line integral $\int dl/B$ over the flux surface, and the prime denotes the derivative with respect to a minor radius flux surface label.) This basic theoretical picture has been substantiated by experiments on the Heliotron-E device,[9] in which the strong $\iota = 1$ resonance lies on the magnetic hill. When the pressure profile $p(r)$ has a significant gradient at $\iota = 1$, sawtooth oscillations are seen on soft x-ray signals emanating from the plasma, and higher frequency fluctuations with poloidal mode number $m = 1$ and toroidal mode number $n = 1$ are seen on both the soft x-ray and edge poloidal magnetic field ($\tilde{B}_\theta$) signals. These instabilities appear to limit the β that can be achieved in Heliotron-E using peaked pressure profiles.[10]

These interchange modes can be stabilized by the magnetic well produced by the outward magnetic axis shift at finite β (Shafranov shift), and this β self-stabilization effect can open a stable path to the second stability regime. The essential physics of this effect can be seen using the large-aspect-ratio limit of the Mercier criterion for a sheared stellarator configuration,[5]

$$D_M = \frac{S^2}{4} + \frac{\rho}{\iota^2 B^2}\frac{dp}{d\rho} R\left(B^2 V_0'' - \frac{(\rho^3\iota)'}{\rho^3}\Delta_p'\right), \quad (1)$$

where B is the magnetic field, R is the major radius, ρ is a normalized minor radial variable, $S \equiv (\rho/\iota)d\iota/d\rho$ is the shear, V_0'' is the vacuum magnetic well or hill, Δ_p' is the finite-β Shafranov shift produced by the Pfirsch–Schlüter currents, and $D_M > 0$ for stability. In sheared torsatron configurations such as ATF, the Mercier criterion in its full three-dimensional formulation gives the most conservative (i.e., pessimistic) indication of stability and therefore can be used to describe the overall ideal MHD plasma properties.[11,12] Equation (1) shows that as β and the Shafranov shift increase, the magnetic well stabilization term increases in magnitude; this ultimately can lead to β self-stabilization if the magnetic configuration properties are chosen appropriately. The magnetic configuration of the ATF device was optimized to explore this possibility.[7]

ATF is an $\ell = 2$, 12-field-period torsatron with major radius $R_0 = 2.10$ m, average minor radius $\bar{a} = 0.27$ m, magnetic field on axis $B_0 \leqslant 2$ T, central rotational transform $\iota_0 \approx 0.3$, and edge transform $\iota_a \approx 1$. Radial profiles of ι and V' for a nominal ATF vacuum field configuration are illustrated in Fig. 2. There is a magnetic well ($V'' < 0$) in the central region where the shear in ι is low and a magnetic hill in the high-shear region near the plasma edge. The magnetic configuration parameters of ATF—aspect ratio, helical field winding law, and auxiliary poloidal shaping fields—were chosen so that as β increases, the plasma remains stable to interchange modes, thus realizing the direct access path to self-stabilization illustrated in Fig. 1. In addition, sufficient flexibility was provided in the ATF device to test stability boundaries by changing the relative currents in the helical and poloidal field coil sets.

For the relatively broad pressure profiles assumed in the ATF design studies,[7] the β self-stabilization effect should dominate at $\beta_0 \approx 5\%$, as illustrated in the stability diagram in Fig. 3(a). However, electron-beam field mapping during initial operation of ATF in early 1988 revealed substantial magnetic islands (6 cm wide at the $\iota = 1/2$ surface and smaller at other rational surfaces).[13] These islands acted as a magnetic limiter and effectively reduced the plasma radius to $r_p \approx 0.6\bar{a}$, which increased the effective aspect ratio A from 8 to 10 and decreased the effective edge transform to $\iota_a \approx 0.5$. This led to a large increase in the Shafranov shift ($\delta/a \propto \beta_0 A/\iota_a^2$ at low β) that enhanced the self-stabilization effect and afforded the results reported in Sec. III.

III. STABILITY OF PLASMAS WITH PEAKED PRESSURE PROFILES

Figure 4(a) shows some of the characteristics of a typical ATF discharge.[6,14] Up to 1.4 MW of H^0 power was injected from co- and/or counteroriented neutral beams into a H^+ target plasma produced with second-harmonic electron cyclotron heating (ECH) using a 0.2 MW, 53 GHz gyrotron at $B_0 = 0.95$ T. The plasma current ranges from near zero for balanced neutral beam injection (NBI) to a maximum of 4.2 kA for unidirectional NBI, but the general characteristics of the discharge do not depend strongly on beam configuration. The volume-average β, defined using the full plasma radius $\bar{a} = 0.27$ m, reached $\langle\beta\rangle = 0.5\%$ at a line-average electron density $\bar{n}_e \approx 2.5\times10^{19}$ m^{-3}, central density $n_{e0} \approx 5\times10^{19}$ m^{-3}, central electron temperature $T_{e0} \approx 0.6$ keV, and ion temperature $T_{i0} \approx 0.26$ keV at $t = 0.265$ sec in

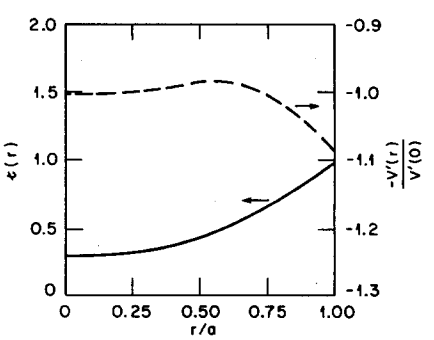

FIG. 2. Radial profiles of rotational transform and specific volume V' for a nominal ATF vacuum field configuration. The central portion of the plasma lies in a magnetic well ($V'' < 0$), while the outer portion lies on a magnetic hill ($V'' > 0$).

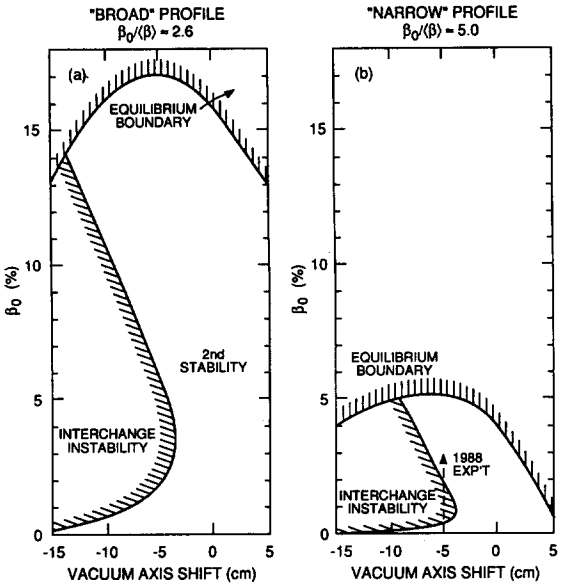

FIG. 3. Stability diagrams for ATF plasmas illustrating the effect of pressure-profile shape.

Fig. 4(a). For this case, the central β is $\beta_0 \approx 3\%$ [Fig. 4(a)], and the global energy confinement time $\tau_E^* \approx 5$ msec. Figure 4(b) shows the T_e profile; the data are plotted in flux coordinates for which ρ is the mean plasma radius normalized to $\bar{a}$. Similarly narrow T_e profiles were observed in both ECH and NBI phases and are believed to have been caused by the islands at $\iota \geqslant 1/2$.

The outward Shafranov shift was large for relatively low values of β: $\delta = 0.11$ m $\approx 2r_p/3$ for $\beta_0 = 3\%$. Such a large shift lowers the ultimate equilibrium β limit, but also lowers the β_c at which self-stabilization becomes dominant. This situation is illustrated in Fig. 3(b), which shows that a more peaked $p(r)$ compresses the stability diagram to lower values of β.

Some of the features of the stability boundaries shown in Fig. 3(b) were immediately evident during the experiments. When the vacuum axis shift was adjusted to $\Delta_V < -10$ cm (plasma pushed inward), the ECH target plasma exhibited gross relaxation oscillations in electron density that limited the plasma parameters to such low values that NBI was not possible. This is consistent with the theoretical picture shown in Fig. 3: a strong inward shift of the magnetic axis eliminates the vacuum magnetic well, and the resulting instability limits the plasma pressure to very low values. Optimum plasma performance was obtained for $\Delta_V = -5$ cm, and these plasmas were used in the stability studies described below. The plasma parameters deteriorated again for $\Delta_V > 0$, probably because the shear decreased and the vacuum field islands increased in size.[14]

Although the field errors constricted the plasma pressure profile $p(\rho)$, there was evidence of systematic changes in $p(\rho)$ as β increased. We define a parameter $\langle\beta\rangle/\bar{n}_e T_{e0}$ as a convenient measure of the "broadness" of the profile. Figure 5(a) shows this parameter as a function of $\langle\beta\rangle$ for the discharges analyzed in the fluctuation studies described below. The pressure profiles broaden substantially as $\langle\beta\rangle$ increases to $\sim 0.2\%$. The time histories of the broadness for individual discharges show a similar dependence on β.

Fluctuation measurements[6] on ATF were made with a soft x-ray detector array viewing the central portion of the plasma ($\rho \leqslant 0.5$) and, for poloidal magnetic fluctuations ($\tilde{B}_\theta$), Mirnov coils located ≈ 30 cm outside the plasma. The soft x-ray signals show no evidence of instabilities. Spectral correlation analysis of the $\tilde{B}_\theta$ signals reveals bands of high-coherence fluctuations (frequency-resolved coherence function > 0.7 even at the largest coil separations; perfect correlation would yield a coherence of 1.0) in the frequency range 5–60 kHz with amplitudes $\sim 10^{-3}$ G. The $\tilde{B}_\theta$ data show predominantly $n = 1$ toroidal mode symmetry. Assignment of poloidal mode numbers (m) to the $n = 1$ fluctuations is complicated by the noncircular flux surface shape and strong Shafranov shift. The data can be interpreted most simply in terms of two principal components, $m = 2$ in the frequency range 5–20 kHz and $m = 3$ in the range 20–45 kHz.

Figure 6 shows the rms coherent $n = 1$ component of $\tilde{B}_\theta$ in the frequency range 5–60 kHz (determined during ECH and at peak β during NBI), plotted as a function of $\langle\beta\rangle$ for a sequence of discharges. The amplitude limit curve of the data suggests that $\langle\tilde{B}(n=1)\rangle$ rises with β for $\langle\beta\rangle \leqslant 0.2\%$, but then saturates and begins to decrease as $\langle\beta\rangle$ exceeds 0.3%. Of course, the trajectory of a given discharge in the $\langle\tilde{B}\rangle$ vs $\langle\beta\rangle$ space of Fig. 6 depends on the evolution of profiles, etc., and this is likely to be the cause of the scatter in the

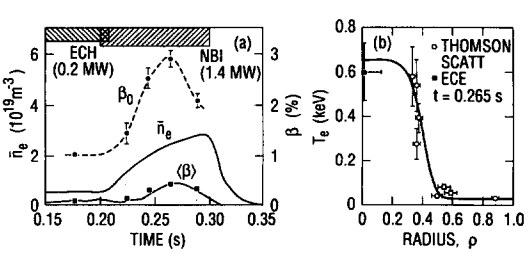

FIG. 4. (a) Time history of an ATF discharge. For the $\langle\beta\rangle$ curve, the smooth trace represents the diamagnetic measurement, and the solid points come from the profile analysis. (b) Electron temperature profile.

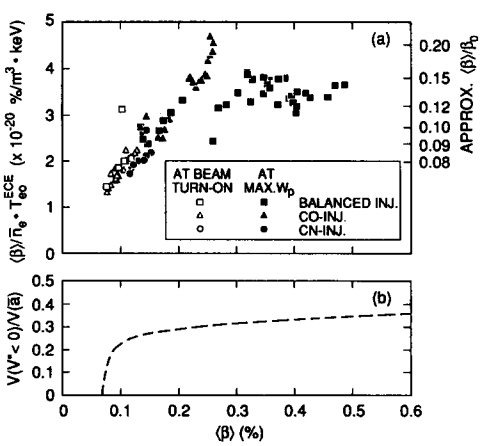

FIG. 5. (a) Profile broadening parameter $\langle\beta\rangle/\bar{n}_e T_{e0}$ vs $\langle\beta\rangle$ for the discharges shown in Fig. 6, and (b) calculated volume of the region of the plasma with $V'' < 0$ (magnetic well).

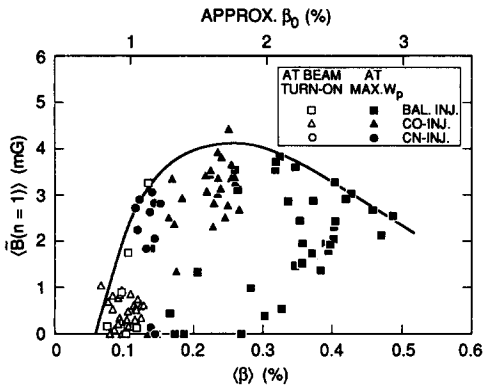

FIG. 6. Dependence of rms (in the frequency band 5–60 kHz) coherent $n = 1$ poloidal magnetic fluctuation amplitude, $\langle\tilde{B}(n=1)\rangle$, on $\langle\beta\rangle$.

data. The time histories of $\langle\tilde{B}\rangle$ in individual discharges in which $\langle\beta\rangle$ exceeds 0.3% recapitulate the curve in Fig. 6; $\langle\tilde{B}\rangle$ rises proportionally with $\langle\beta\rangle$ for $\langle\beta\rangle < 0.3\%$ and then decreases as $\langle\beta\rangle$ exceeds this value.

Additional trend analyses of $\langle\tilde{B}\rangle$ show no obvious additional correlations of the magnetic fluctuations with plasma current, fast-ion pressure, or fast-ion density.

Theoretical studies[6,12] of the ideal MHD stability of ATF plasmas with peaked profiles showed that if the shape of $p(\rho)$ is fixed to have the shape measured in the experiment at high β [Fig. 4(b)], and a series of equilibria of successively higher β is calculated, the plasma passes through a Mercier unstable region in the range $\langle\beta\rangle = 0.01\%$–$0.3\%$, whereupon it enters the ideal second stability regime. Equilibria from a second series of calculations in which $p(\rho)$ was allowed to evolve with β along the path indicated in the experiment [Fig. 5(a)] were found to be Mercier stable, suggesting that the plasma remains close to marginal stability along the path to second stability.

Multiple-helicity resistive turbulence calculations[12,15] were carried out to examine the stability of dissipative modes and in particular resistive interchange modes, which remain unstable even in the ideal MHD second stability regime. The results show that the plasma pressure contours become progressively more disturbed as $\langle\beta\rangle$ increases to $\approx 0.3\%$ and smooth out at higher β as the turbulence is reduced by the β self-stabilization effect.

The nonlinear calculations show that the $\tilde{B}_\theta$ spectrum at the plasma edge is dominated by the lowest n modes ($n = 1$, $m = 2$ and $n = 1$, $m = 3$). The amplitude of the $n = 1$ component of $\tilde{B}$ increases with $\langle\beta\rangle$ for $\langle\beta\rangle < 0.38\%$ and decreases as $\langle\beta\rangle$ exceeds this value. These features are similar to those observed in the experiment, but the experimental values of $\tilde{B}/B \sim 10^{-6}$ inferred at the plasma edge of the experiment are smaller (by a factor > 10) than those from the nonlinear calculations, which may imply that other stabilizing effects (such as ω^* and other kinetic effects) should be included in the modeling or that the radial decay of $\tilde{B}$ outside the plasma is faster than that expected from a simplified vacuum field solution.

The β self-stabilization results from the radial expansion of the region with magnetic well ($V'' < 0$), coupled with an increase in the magnitude of the favorable V''. The calculated $\langle\beta\rangle$ dependence of the volume of the magnetic well [Fig. 5(b)] is similar to that of the pressure-profile broadening observed in the experiment. This similarity could be evidence of improved plasma confinement due to stabilization, but measurements connecting local transport and fluctuations are needed to substantiate this interpretation further. Analysis of *global* confinement data for these discharges shows that the global energy confinement time apparently increases at high β, but the close coupling of density and β in these NBI-heated plasmas makes it difficult to separate out β effects.[14]

IV. INITIAL RESULTS FOR PLASMAS WITH BROAD PROFILES

In 1989, the field error in ATF (which was caused by an asymmetry in the coil current feeds) was removed,[13] and the gettering system was improved. Operation during 1989 has also been mainly at $B_0 = 1.9$ T. While these simultaneous changes make precise comparison of results difficult, the changes in plasma behavior that have been observed are nonetheless striking. Additional details on plasma performance in these experiments are available in Ref. 16.

Figure 7 compares sample electron temperature and density profiles obtained before and after the field error was repaired. The profiles measured in the absence of the field error show significant gradients outside the former location of the $\iota = 1/2$ island at $\rho = 0.6$; it is clear that the pressure profile is now significantly broader.

Initial analysis of Mirnov coil data has been carried out for a broad sample set of the discharges obtained after the field error repair. Poloidal and toroidal mode spectra for $\tilde{B}_\theta$ were determined with the same coherence techniques that were used in the initial second stability experiments. Figure 8 compares the mode spectra observed before and after the

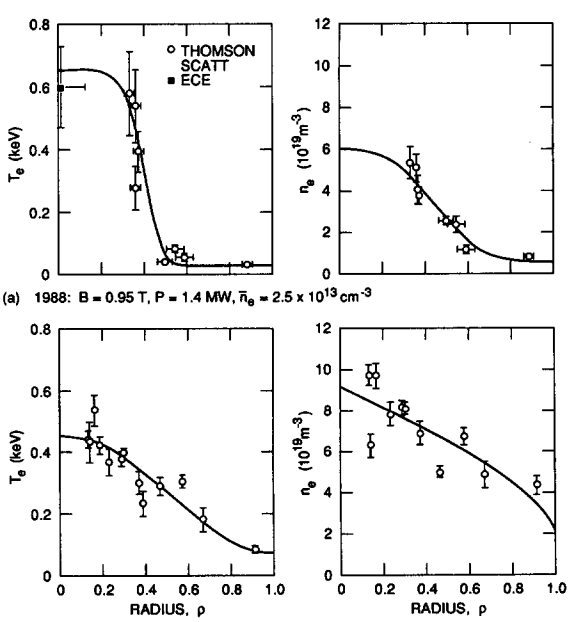

FIG. 7. ATF electron temperature and density profiles (a) before and (b) after repair of field error.

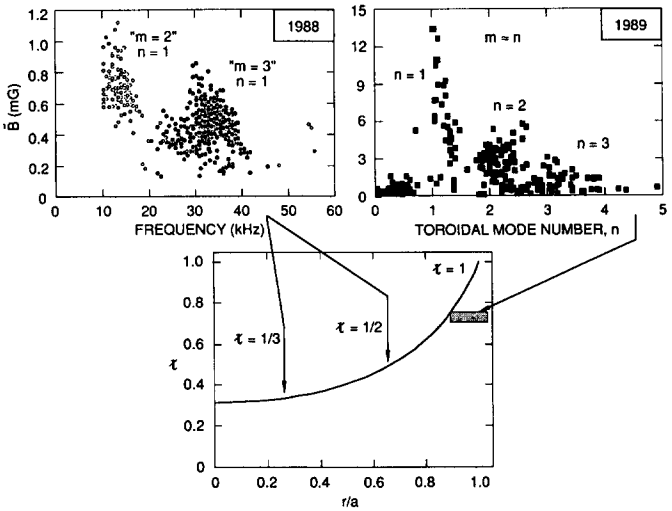

FIG. 8. Diagram summarizing mode numbers observed for magnetic fluctuations before repair of the field error [1988—peaked $p(r)$] and after repair of the field error [1989—broad $p(r)$].

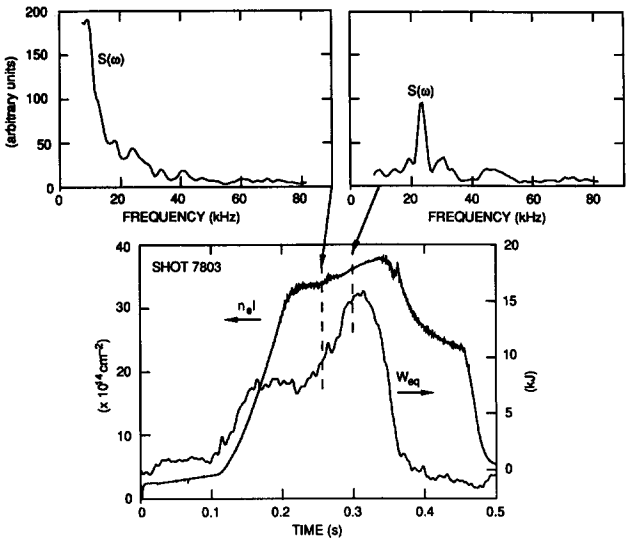

FIG. 9. Correlation of change in edge density fluctuation power spectra $S(\omega)$ with improvement in global energy confinement. The time traces show the chordal electron density ($n_e l$) and the stored energy (W_{eq}) determined from poloidal magnetic field measurements. The fluctuation spectra were measured at $r/a \approx 0.9$ using microwave reflectometry at 33 GHz (cutoff density $= 1.35 \times 10^{13}$ cm^{-3}). The spectra were averaged over 12.5 msec intervals centered at the times indicated. The NBI power (balanced injection) was 1.4 MW.

field error repair. Before the repair, the $\tilde{B}_\theta$ spectra showed two distinct modes—($m = 2, n = 1$) and ($m = 3, n = 1$)—that were clearly separated in frequency, as shown in the plot in the upper left corner of Fig. 8. Data taken after the field error repair[17] show modes of different m and n overlapping in frequency, with both m and n increasing with frequency. For the bulk of the data, $n/m \gtrsim 1$, indicating that the modes resonate at or even slightly outside the nominal plasma boundary at $\iota = 1$; this observation is consistent with the general broadening of the pressure profile: the shift of ∇p to larger minor radii would presumably drive modes that are resonant at higher ι. Since the modes are not now clearly separated in frequency, the amplitudes are plotted as a function of toroidal mode number in the plot on the upper right of Fig. 8. The amplitudes are in general larger than before the field error repair; this is also a consequence of the shift in the resonances to radii of higher ι, which are closer to the Mirnov coils. Note that no attempt has been made to correct for the vacuum field decay of $\tilde{B}_\theta$ outside the plasma. In a simple cylindrical approximation, $\tilde{B}_\theta(r) \propto r^{-(m+1)}$; thus, for $m \sim n$, the amplitudes of the high-n ($n \geqslant 3$) modes now observed are comparable to or greater than those of the low-n modes.

A microwave reflectometer system has been used to make initial measurements of edge density fluctuations in these plasmas.[18] While exact determination of $\tilde{n}/n$ using this method is difficult and requires careful modeling, qualitative features of the fluctuation spectrum can be discerned readily.

Figure 9 illustrates data from a representative discharge obtained after the field error repair. After NBI is turned on at $t = 0.1$ sec, the plasma stored energy rises quickly and then remains constant until $t \approx 0.25$ sec, when the gas fueling is significantly reduced. During this time, the density fluctuations at $r/a = 0.9$ as measured with the reflectometer have a broadband spectrum that has a maximum at low frequencies ≈ 10 kHz. The chordal electron density ($n_e l$), which is low-pass filtered at 10 kHz, also shows fluctuations.

At $t \approx 0.25$ sec, the plasma behavior changes dramatically. The stored energy W_{eq} increases by a factor of 2 or more; the NBI power remains approximately constant until $t \approx 0.45$ sec, so the increase in W_{eq} corresponds to an increase in τ_E^*. Thomson scattering measurements indicate that T_{e0} increases by only $\sim 20\%$; thus, the increase in stored energy appears to be primarily due to a broadening of the pressure profile. The $\tilde{n}$ spectrum measured with the reflectometer changes to a narrow-band spectrum with a strong peak between 20 and 40 kHz. The decrease in low-frequency fluctuations is also seen in the $n_e l$ signal. The narrow-band component of $\tilde{n}$ is coherent with $\tilde{B}_\theta$ as measured by the Mirnov coils, and analysis of the Mirnov coil data shows that the coherent $\tilde{B}_\theta$ components have toroidal mode numbers $n \geqslant 3$. Analysis of reflectometer data from discharges at $B_0 = 0.95$ and 1.9 T and at various densities indicates that the signature change in the $\tilde{n}$ spectrum occurs at $\langle \beta \rangle = 0.1\%$–$0.2\%$.

Explanation of this transition in plasma behavior will require significant further experimentation and analysis, but it is possible to speculate about the physical mechanisms that may be involved. The sharp change in edge fluctuation behavior reflects a change in the stability of the plasma and/or in the turbulence characteristics. Stabilization could be either a cause or an effect of the broadening of the pressure profile. The change in the frequency spectrum may also be evidence of a change in the structure of the radial electric field, since fluctuations in stellarators and tokamaks are Doppler shifted by the $\mathbf{E} \times \mathbf{B}$ drift. Other experiments suggest that radial electric fields and poloidal flow are important in stellarators[19] and in the L–H transition in tokamaks.[20]

V. CONCLUSIONS

Access to the second stability regime has been achieved in ATF using peaked pressure profiles. The experimental β values (up to 3%) are well above the theoretically predicted transition to second stability at $\beta_0 \approx 1.3\%$. The measured magnetic fluctuations show evidence of β self-stabilization and are consistent with theoretical predictions for resistive interchange modes. The pressure profile broadens with increasing β and the plasma appears to remain near ideal MHD marginal stability along the path to second stability.

Initial operation with broad pressure profiles shows instabilities shifting toward the plasma edge, and a transition to improved confinement that is signaled by a marked change in edge fluctuation characteristics.

ACKNOWLEDGMENTS

We acknowledge with appreciation the continual support of R. A. Dory, M. J. Saltmarsh, and J. Sheffield.

This research was sponsored by the Office of Fusion Energy, U.S. Department of Energy, under Contract No. DE-AC05-84OR21400 with Martin Marietta Energy Systems, Inc.

[1] A. B. Mikhailovskii and V. D. Shafranov, Sov. Phys. JETP **39**, 88 (1974).
[2] B. Coppi, A. Ferreira, J. W.-K. Mark, and J. J. Ramos, Nucl. Fusion **19**, 715 (1979).
[3] L. M. Kovrizhnykh and S. V. Shchepetov, Sov. J. Plasma Phys. **6**, 533 (1980).
[4] S. C. Luckhardt, K.-I. Chen, S. Coda, J. Kesner, R. Kirkwood, B. Lane, M. Porkolab, and J. Squire, Phys. Rev. Lett. **62**, 1508 (1989).
[5] V. D. Shafranov, Phys. Fluids **26**, 357 (1983).
[6] J. H. Harris, M. Murakami, B. A. Carreras, J. D. Bell, G. L. Bell, T. S. Bigelow, L. A. Charlton, N. Dominguez, J. L. Dunlap, J. C. Glowienka, L. D. Horton, H. C. Howe, R. C. Isler, H. Kaneko, R. R. Kindsfather, J. N. Leboeuf, V. E. Lynch, M. M. Menon, R. N. Morris, G. H. Neilson, V. K. Paré, D. A. Rasmussen, J. B. Wilgen, and W. R. Wing, Phys. Rev. Lett. **63**, 1249 (1989).
[7] J. F. Lyon, B. A. Carreras, K. K. Chipley, M. J. Cole, J. H. Harris, T. C. Jernigan, R. L. Johnson, V. E. Lynch, B. E. Nelson, J. A. Rome, J. Sheffield, and P. B. Thompson, Fusion Technol. **10**, 179 (1986).
[8] M. S. Chance, S. C. Jardin, and T. H. Stix, Phys. Rev. Lett. **51**, 1963 (1983).
[9] J. H. Harris, O. Motojima, H. Kaneko, S. Besshou, H. Zushi, M. Wakatani, F. Sano, S. Sudo, A. Sasaki, K. Kondo, M. Sato, T. Mutoh, T. Mizuuchi, M. Iima, T. Obiki, A. Iyoshi, and K. Uo, Phys. Rev. Lett. **53**, 2242 (1984).
[10] H. Zushi, O. Motojima, M. Wakatani, F. Sano, S. Sudo, H. Kaneko, K. Kondo, T. Mizuuchi, K. Yaguchi, M. Sato, A. Iiyoshi, and K. Uo, Nucl. Fusion **27**, 895 (1987).
[11] N. Dominguez, J. N. Leboeuf, B. A. Carreras, and V. E. Lynch, Nucl. Fusion **29**, 2079 (1989).
[12] See National Technical Information Service Document No. DE 89 013737/JAW (Oak Ridge National Laboratory Report No. ORNL/TM-11102 by B. A. Carreras *et al.*). Copies may be ordered from the National Technical Information Service, Springfield, VA 22181. The price is $12.95 plus $3.00 handling fee. All orders must be prepaid.
[13] J. H. Harris, T. C. Jernigan, F. S. B. Anderson, R. D. Benson, R. J. Colchin, M. J. Cole, A. C. England, R. F. Gandy, M. A. Henderson, D. L. Hillis, R. L. Johnson, D. K. Lee, J. F. Lyon, G. H. Neilson, B. E. Nelson, J. A. Rome, M. J. Saltmarsh, C. W. Simpson, D. J. Taylor, P. B. Thompson, and J. C. Whitson, Fusion Technol. **17**, 51 (1990).
[14] M. Murakami, B. A. Carreras, J. H. Harris, F. S. B. Anderson, G. L. Bell, J. D. Bell, T. S. Bigelow, R. J. Colchin, E. C. Crume, N. Dominguez, J. L. Dunlap, A. C. England, J. C. Glowienka, L. D. Horton, H. C. Howe, R. C. Isler, H. Kaneko, R. R. Kindsfather, J. N. Leboeuf, V. E. Lynch, M. M. Menon, R. N. Morris, G. H. Neilson, V. K. Paré, D. A. Rasmussen, J. B. Wilgen, and W. R. Wing, in *Proceedings of the 16th European Conference on Controlled Fusion and Plasma Physics,* Venice, 1989 (European Physical Society, Geneva, 1989), Vol. 13B, Part II, p. 575.
[15] L. A. Charlton, J. N. Leboeuf, B. A. Carreras, and V. E. Lynch, Bull. Am. Phys. Soc. **34**, 2059 (1989).
[16] R. J. Colchin, M. Murakami, E. Anabitarte, F. S. B. Anderson, G. L. Bell, J. D. Bell, T. S. Bigelow, E. C. Crume, J. L. Dunlap, G. R. Dyer, A. C. England, P. W. Fisher, W. A. Gabbard, J. C. Glowienka, R. H. Goulding, J. W. Halliwell, G. R. Hanson, J. H. Harris, G. R. Haste, C. Hidalgo-Vera, D. L. Hillis, S. Hiroe, L. D. Horton, H. C. Howe, D. E. Hutchinson, R. C. Isler, T. C. Jernigan, M. Kwon, R. A. Langley, D. K. Lee, J. F. Lyon, J. W. Lue, C. H. Ma, M. M. Menon, R. N. Morris, P. K. Mioduszewski, G. H. Neilson, A. L. Qualls, D. A. Rasmussen, P. S. Rogers, P. L. Shaw, T. D. Shepard, J. E. Simpkins, S. Sudo, C. E. Thomas, T. Uckan, M. R. Wade, J. B. Wilgen, W. R. Wing, H. Yamada, and J. J. Zielinski, Phys. Fluids B **2**, Pt. 2, 1348 (1990).
[17] J. D. Bell, J. H. Harris, J. L. Dunlap, and V. K. Paré, Bull. Am. Phys. Soc. **34**, 1948 (1989).
[18] G. R. Hanson, E. Anabitarte, C. E. Thomas, J. H. Harris, and J. B. Wilgen, Bull. Am. Phys. Soc. **34**, 1948 (1989).
[19] B. A. Carreras, G. Grieger, J. H. Harris, J. L. Johnson, J. F. Lyon. O. Motojima, F. Rau, H. Renner, J. A. Rome, K. Uo, M. Wakatani, and H. Wobig, Nucl. Fusion **28**, 1613 (1988).
[20] K. H. Burrell, Bull. Am. Phys. Soc. **34**, 2073 (1989).